Available online at www.sciencedirect.com
ScienceDirect
Scripta Materialia xxx (2014) xxx–xxx
Scripta MATERIALIA
www.elsevier.com/locate/scriptamat

In situ transmission electron microscopy observations of room-temperature plasticity in sub-micron-size TaC(100) and TaC(011) single crystals

Q1 S. Kiani,[a] C. Ratsch,[b] A.M. Minor,[c] J.-M. Yang[a,*] and S. Kodambaka[a,*]

[a]*Department of Materials Science and Engineering, University of California Los Angeles, Los Angeles, CA 90095, USA*
[b]*Department of Mathematics and Institute for Pure and Applied Mathematics, University of California Los Angeles, Los Angeles, CA 90095, USA*
[c]*Department of Materials Science and Engineering, University of California Berkeley and National Center for Electron Microscopy, Lawrence Berkeley National Laboratory, Berkeley, CA 94720, USA*

Received 1 September 2014; revised 25 November 2014; accepted 30 November 2014

Using in situ electron microscopy based uniaxial compression and density functional theory calculations, we investigated the room-temperature mechanical responses of sub-micron-scale cylindrical TaC(100) and TaC(011) pillars. The TaC(100) and TaC(011) pillars deform plastically via shear along $\{1\bar{1}0\}\langle 110\rangle$ and $\{1\bar{1}1\}\langle 110\rangle$, respectively. Interestingly, both TaC(100) and TaC(011) exhibit size-independent yield strengths, with average values of 9 ± 2.4 and 11 ± 3.4 GPa, respectively. Our results provide new insights into the role of crystal anisotropy on room-temperature plasticity in TaC.

Keywords: Refractory carbides; Tantalum carbide; Room-temperature plasticity; In situ transmission electron microscopy; Slip systems

Refractory transition-metal carbides (TMC) and nitrides [1–3], owing to a combination of strong ionic, covalent and metallic bonds, possess good thermomechanical properties, along with good resistance to ablation, corrosion and wear. They are thus attractive for applications in cutting tools, as wear- and oxidation-resistant coatings, as structural components (leading edges and nose-caps) in hypersonic vehicles, as diffusion barriers, as electrical conductors and as optical thin films [4–7]. Among the group IV and V binary TMCs with a rocksalt (B1) structure, tantalum carbide (TaC) has one of the highest melting points (T_m 4250 K) [1] and electrical conductivities (>5×10^{6} $^{-1}$ m^{-1} at 300 K) [1,3]. Its mechanical properties are sensitive to carbon content [4–6] and comparable to those of other TMCs: TaC is stiff (elastic modulus ~537 GPa) [1], moderately hard (10 s of GPa) [2,7] and, although localized plasticity is observed under microindents at room temperature [7–9], macroscopic ductility is more pronounced at temperatures $0.5T_m$ [4,5]. Room-temperature microindentation studies revealed that $\{1\bar{1}1\}\langle 110\rangle$ is the most commonly observed slip system in TaC [8,9]. However, the existing data on slip systems operating at elevated temperatures are conflicting: Rowcliffe and Warren reported that, at 1470 K, slip can occur along $\{001\}$ or $\{011\}$ [8], while others have indicated that $\{1\bar{1}1\}\langle 110\rangle$ is the slip system operating at all temperatures [9,10].

Among the TMCs, the mechanical behavior of TaC is probably unique: single crystals of TaC were shown to deform plastically, rather than crack, during microindentation at temperatures as low as 77 K. This unexpected observation was attributed to the activation of a second slip system $\{1\bar{1}0\}\langle 110\rangle$ at 77 K in addition to the commonly expected $\{1\bar{1}1\}\langle 110\rangle$ [7]. The hardness of B1-structured TaC_x was found to be maximum at an intermediate (x 0.8), rather than a higher/lower ($x = 0.5$ or 1), carbon vacancy concentration [2,5,8]. The hardness of TaC was found to decrease gradually, rather than abruptly, with increasing temperature [10]. Considerable (~90%) densification of TaC powders was achievable using >7 GPa pressures at room temperature, and this was attributed to dislocation motion along multiple orientations, the formation of nanotwins and the rotation of grains [11]. All of these results suggest that TaC is likely to be more metallic [10] and tougher than other B1-structured binary TMCs [7]. The operation of multiple slip systems and the observation of plastic flow at room temperature in polycrystalline TaC point to the possibility of realizing "ductile ceramics", i.e. the combination of high hardness and ductility. The availability of such materials would lead to improvements in damage tolerance of structural components and could potentially also open up new applications in extreme

* Corresponding authors. e-mail addresses: jyang@seas.ucla.edu; kodambaka@ucla.edu

http://dx.doi.org/10.1016/j.scriptamat.2014.11.036
1359-6462/

environments. Achieving this goal in the class of TMCs is not a trivial task, and at minimum would require detailed knowledge of the roles of composition, slip systems, crystal anisotropy and structural defects such as dislocations on the deformation behavior of the TMCs. For TaC, while previous studies have provided some insights into the effects of composition and the slip systems that operate during indentation, relatively little is known concerning the factors affecting room-temperature plasticity. Here, as a first step, we focus on addressing the role of crystal anisotropy using a combination of in situ transmission electron microscopy (TEM) based uniaxial compression tests and density functional theory (DFT) calculations of deformation of TaC(100) and TaC(011) single crystals.

All of our in situ compression experiments were carried out using cylindrical TaC pillars prepared via focused ion beam (FIB) milling of TaC(100) and TaC(011) single crystals (nominal composition $\sim TaC_{0.85}$, 2 mm thick, 2 mm diameter circular disks, from Applied Physics Technologies). The pillar fabrication process is described in detail in Ref. [12]. Briefly, the bulk crystals are first cut into two halves, one of which is mechanically polished to sub-100 μm thickness. The thinned samples are then mounted on transmission electron microscope stubs and transferred to an FEI 235 FIB system. Pillars of diameters D between 0.1 and 0.5 μm with aspect ratios of 1.5–3.3, chosen to minimize buckling, are prepared using 30 kV Ga + beams in two steps. Initial coarse milling is carried out at an ion beam current of 20 nA, followed by fine milling with a 30 pA current. This milling procedure yields pillars with a slightly tapered (<3°) geometry.

The in situ compression tests were carried out using a Hysitron TEM PicoIndenter 95 with a flat 3 μm wide diamond punch in a JEOL 3010 transmission electron microscope operated at 300 kV. Each of the TaC(100) and TaC(011) pillars is uniaxially compressed along [100] and [011], respectively, in displacement-control mode at a constant loading rate of 4 nm s^{-1}. During each test, load–displacement data, video-rate (30 frames s^{-1}) TEM images and selected area electron diffraction (SAED) patterns are acquired.

Using DFT, we calculated the energy barriers associated with slip and shear in stoichiometric, defect-free, TaC single crystals along different slip systems composed of the three low-index planes, (100), (110) and (111), and the directions ⟨100⟩, ⟨110⟩ and ⟨111⟩. All of our DFT calculations are performed with the FHI-AIMS code [13] using supercells with periodic boundary conditions and GGA-PBE for the exchange–correlation functional [14]. The slab consisted of at least 12 layers that are periodic in the x and y directions and separated by at least 30 Å of vacuum along the z direction. We carefully tested the convergence of our results with respect to the slab and vacuum layer thicknesses, the basis set and the density of the (numerical) integration mesh.

For each slip system, we determined the unstable stacking fault energy, a measure of the resistance to dislocation nucleation in an otherwise perfect crystal [15]. To this purpose, we first calculated the generalized stacking fault energy E_{GSF} as a function of normalized displacement (x/**b**), where **b** is the Burgers vector for that slip direction. $E_{GSF}(x)$ is defined as the energy per unit area required to shift one half of the supercell with respect to the other half by a distance x. In all the calculations, the top half of the slab is moved uniformly along the desired slip direction until we reach a saddle point; all the atoms are constrained along the slip direction but fully relaxed in the other directions. We then obtain the unstable stacking fault energy as the maximum value in the E_{GSF} vs. (x/**b**) curve.

We also calculated the total energy per unit volume required to induce shear strain along the three primary slip systems, $\{001\}\langle 110\rangle$, $\{1\bar{1}0\}\langle 110\rangle$ and $\{1\bar{1}1\}\langle 110\rangle$. In these calculations, the entire slab is sheared. That is, we move the first layer a certain distance dx, until it reaches a saddle point. During shear, we then move the second layer by 2dx, the third layer by 3dx, etc. This is in contrast to the above description of the slippage, where the entire upper half of the slab is moved by dx. As a consequence, the more layers we consider, the higher the absolute energy barrier. Therefore, we normalize the energy for shear per unit volume.

Figure 1(a)–(d) are representative bright-field TEM images extracted from a video (see "TaC(100) movie") recorded during compression of an ~0.45 μm long TaC(100) pillar with $D = 0.13$ μm. In this experiment, we observe localized deformation and the formation of shear bands near the top of the pillar that is in contact with the diamond punch. The first occurrence of slip, labeled 1 in Figure 1(b), is observed at ~10 GPa of applied stress, corresponding to ~35 nm of displacement, and is followed by the formation of a surface step. Upon further compression, a second shear event, labeled 2 in Figure 1(b), appears at a displacement of ~50 nm associated with an applied stress of ~13.5 GPa. Figure 1(c) shows the post-compression morphology of the pillar. The SAED pattern (inset in Fig. 1(c)) acquired from the compressed pillar indicates that the pillar retains its single crystalline B1 structure and does not undergo phase transformation or twinning. Figure 1(d) is a representative plot of stress vs. displacement measured during in situ compression of the TaC(100) pillar. The pillar deforms elastically during the initial stages of compression, while the measured displacement increases linearly with the applied stress. With increasing stress above the yield strength (σ_y), the pillar deforms plastically and the displacement varies non-linearly with the applied stress. In order to determine σ_y, the stress–displacement data are plotted on a log–log scale and linear least-squares fits are used to identify the yield point at which the slope of the curve changes. In this experiment, the transition from elastic to plastic deformation occurred at an engineering stress, i.e. σ_y 10 GPa.

From the analyses of SAED pattern (inset in Fig. 1(c)) and the projected direction of the shear traces observed in the TEM image (Fig. 1(c)), we determined that the normal to the shear traces passes through the $(2\bar{2}0)$ planes, i.e. the orientation of slip planes is $\{1\bar{1}0\}$. Assuming that ⟨110⟩, the direction with the shortest repeat distance in B1 lattice, is also the slip direction in TaC [8,9], we suggest that the primary slip systems operating during uniaxial compression of TaC(100) pillars are $\{1\bar{1}0\}\langle 110\rangle$. This is plausible since the resolved shear stress is highest (Schmid factor, $\beta = 0.5$) for $\{1\bar{1}0\}\langle 110\rangle$ during compression along [100]. We realize that our result is in contrast with existing reports [7] that identify $\{1\bar{1}1\}\langle 110\rangle$ as the slip system, which could be due to differences in loading: uniaxial stresses in our experiments vs. hydrostatic stresses in indentation.

We find that the TaC(011) pillars subjected to uniaxial compression also exhibit shear deformation, similar to the mechanical response of TaC(100) pillars. Figure 1(e)–(h) are typical bright-field TEM images extracted from a video (see "TaC(011) movie") recorded during the compression of an ~0.45 μm long TaC(011) pillar with $D = 0.115$ μm.

Please cite this article in press as: S. Kiani et al., Scripta Mater. (2014), http://dx.doi.org/10.1016/j.scriptamat.2014.11.036

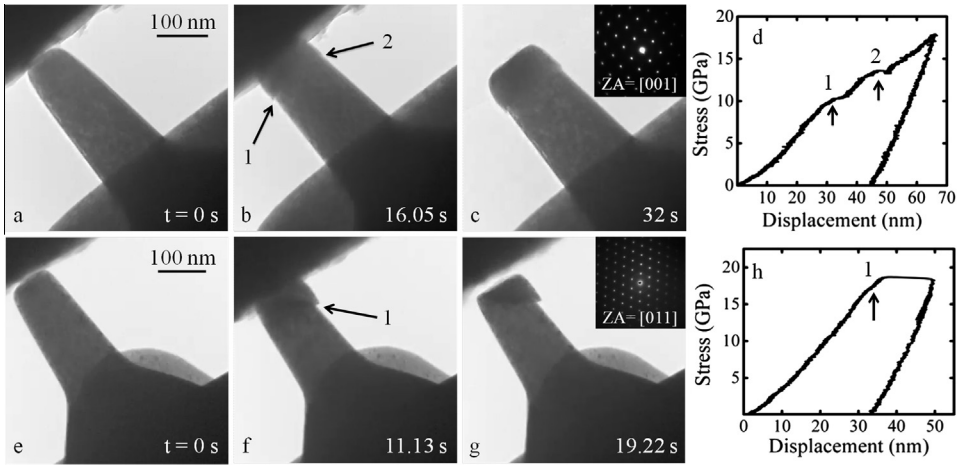

Figure 1. Bright-field TEM images (extracted from "TaC(100) movie" and "TaC(011) movie"), SAED patterns and plots of engineering stress vs. displacement data acquired in situ during displacement-controlled uniaxial compression of (a–d) a TaC(100) pillar with diameter $D = 0.13$ μm and (e–h) a TaC(011) pillar with $D = 0.115$ μm. Images (a, e) show the pillars before and (c, g) after the compression tests. The insets in (c, g) show SAED patterns from the compressed pillars along (c) [001] and (g) [011] zone axes. Labels 1 and 2 in images (b, f) and in the plots (d, h) correspond to displacement bursts resulting from the initiation and propagation of shear planes.

Figure 1(g) shows the post-compression morphology of the pillar, with the corresponding SAED pattern as an inset, which indicates that the pillar deforms plastically while its crystallinity remains intact. In this experiment, the major shear event, labeled 1 in Figure 1(f), occurs at an applied stress of ~17 GPa, corresponding to a displacement of ~35 nm (see the stress vs. displacement plot in Fig. 1(h)), and is followed by the formation of a surface step. From the shear traces observed in the TEM image along with the SAED pattern (Fig. 1(g)), following the procedure similar to that employed for TaC(100) pillars, we identify $\{1\bar{1}1\}$ as the active slip plane. Assuming that $\langle 110\rangle$ is the slip direction, the resolved shear stress during loading along [011] is highest ($\beta = 0.408$) on the $\{1\bar{1}1\}\langle 110\rangle$ slip system compared to the $\{001\}\langle 110\rangle$ ($\beta = 0.353$) and $\{1\bar{1}0\}\langle 110\rangle$ ($\beta = 0.25$) slip systems. Therefore, we suggest that $\{1\bar{1}1\}\langle 110\rangle$ is the active slip system during uniaxial compression of TaC(011) pillars.

Table 1 lists DFT-calculated values of unstable stacking fault energies (the maxima in $E_{GSF}(x)$ curves) and the total energy per unit volume required to shear for several different possible slip systems in TaC. The unstable stacking fault energies, which are measures of resistance to dislocation nucleation, are found to be lowest (0.035 eV Å^{-2}) along $\{1\bar{1}1\}\langle 110\rangle$, followed by 0.103 eV Å^{-2} along $\{1\bar{1}0\}\langle 110\rangle$ and 0.139 eV Å^{-t2} long $\{001\}\langle 110\rangle$. That is, $\{1\bar{1}1\}\langle 110\rangle$ is energetically the most favorable slip system for dislocation nucleation in TaC. The total energy per unit volume required to shear, which is a measure of ideal shear stress, is found to be lowest (0.092 eV Å^{-3}) for $\{001\}\langle 110\rangle$, compared to 0.476 eV Å^{-3} for $\{1\bar{1}1\}\langle 110\rangle$ and 0.492 eV Å^{-3} for $\{1\bar{1}0\}\langle 110\rangle$. We realize that our DFT calculations can only estimate the energies associated with dislocation nucleation in perfect, defect-free crystals. Identifying the dislocation propagation mechanisms and plastic deformation pathways is computationally challenging, as they require significantly large simulation cells (>1000 atoms), multi-scale modeling of dislocation dynamics and knowledge of the interatomic potentials for TaC, and hence are beyond the scope of this letter.

To gain better insights into the plastic deformation behavior in TaC, we carried out uniaxial compression tests

Table 1. DFT calculated values of unstable stacking fault energies and total energies required to shear for TaC along different slip systems.

Slip system	$\{001\}\langle 110\rangle$	$\{1\bar{1}0\}\langle 110\rangle$	$\{1\bar{1}1\}\langle 110\rangle$	$\{001\}\langle 100\rangle$	$\{1\bar{1}0\}\langle 100\rangle$	$\{1\bar{1}0\}\langle 111\rangle$
Max(E_{GSF}), eV/Å^2	0.139	0.103	0.035	0.168	0.309	0.336
Shear energy, eV/Å^3	0.092	0.492	0.476	–	–	–

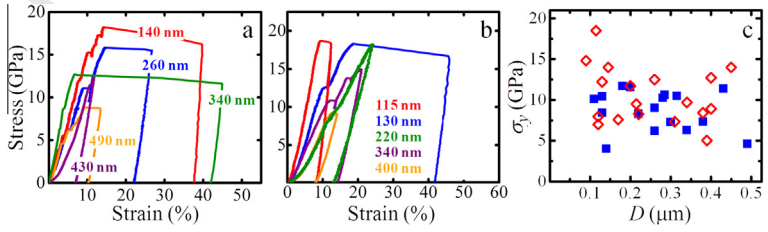

Figure 2. Representative plots of engineering stress vs. engineering strain acquired from (a) TaC(100) and (b) TaC(011) pillars of different D, color-coded for clarity. (c) Plot of yield strengths σ_y vs. D for all the TaC(100) (■) and TaC(◇)) pillars. (For interpretation of the references to colour in this figure legend, the reader is referred to the web version of this article.)

Please cite this article in press as: S. Kiani et al., Scripta Mater. (2014), http://dx.doi.org/10.1016/j.scriptamat.2014.11.036

on a total of 17 TaC(100) and 18 TaC(110) pillars of D between 0.10 and 0.50 μm. Figure 2(a) and (b) are plots of stress–displacement data obtained from (100)- and (011)-oriented pillars with different D, respectively. For a given crystallographic orientation, the deformation behavior of all the pillars is similar to the data presented in Figure 1. We find that the maximum stress withstood by the pillars before failure increases little with decreasing D. From the log–log plots of the stress–displacement data, we determined the yield points and $\sigma_{y,100}$ and $\sigma_{y,011}$ of the TaC(100) and TaC(011) crystals, respectively. Figure 2(c) is a plot of σ_y vs. D for all the TaC pillars. While there is a large scatter of the data, within the measurement uncertainties, both $\sigma_{y,100}$ and $\sigma_{y,011}$ appear to vary little with D. We find that the average yield strengths are $\sigma_{y,100} = 9 \pm 2.4$ GPa and $\sigma_{y,011} = 11 \pm 3.4$ GPa. That is, TaC(100) is relatively softer, under uniaxial compression, than TaC(011). The size-invariant σ_y observed in TaC(100) and TaC(011) crystals suggests that neither $\{1\bar{1}0\}\langle 110\rangle$ nor $\{1\bar{1}1\}\langle 110\rangle$ is the "soft" slip system in TaC [16].

In our experiments, those slip systems with the highest , i.e. $\{1\bar{1}0\}\langle 110\rangle$ and $\{1\bar{1}1\}\langle 110\rangle$, are found to operate during uniaxial loading along [100] and [011], respectively, while the DFT calculations suggest that $\{1\bar{1}1\}\langle 110\rangle$ is the preferred slip system for dislocation nucleation. Also, the absence of size-dependence in the measured σ_y values suggests that dislocation density, which is expected to increase with increasing D, has little effect on σ_y. Based upon these results, we speculate that dislocation motion, rather than nucleation, along $\{1\bar{1}0\}\langle 110\rangle$ and $\{1\bar{1}1\}\langle 110\rangle$ controls the plastic deformation in TaC(100) and TaC(011) crystals, respectively. While our conclusion is consistent with that presented in earlier reports [5,9], we realize that pillar geometry can influence the size-dependences in σ_y [17]. Therefore, further investigation (e.g. measurements of σ_y using untapered pillars [18], analyses of dislocation structure and number density in the pillars before and after compression) is necessary to validate our hypothesis.

The observed (or lack of) size- and orientation-dependent mechanical behavior of B1-structured TaC is strikingly different from that observed in ionic compounds such as MgO [14] and LiF [12,13] and the highly anisotropic size-dependent yield strengths found in ZrC [19], another B1-structured TMC. Such a difference is not unexpected, given that the nature and relative strengths of metal–metal and metal–carbon bonds vary with the valence electron concentration in the lattice [20] and the covalent radii of the metal cations. Nevertheless, the phenomenon of room-temperature plasticity in ZrC and, through the results presented here, in TaC provide further evidence for the hypothesis presented over five decades ago [21] that NaCl-structured crystals can also be ductile at room temperature, at least in sub-micron-scale crystals.

In summary, we investigated the room-temperature mechanical behavior of TaC(100) and TaC(011) crystals subjected to uniaxial compression using a combination of in situ electron microscopy and DFT calculations. We find that TaC crystals undergo shear deformation and that their yield strengths vary little with crystal size. The measurements of yield strength as a function of crystal orientation reveal that the slip systems with the highest resolved shear stresses, i.e. $\{1\bar{1}0\}\langle 110\rangle$ in TaC(100) and $\{1\bar{1}1\}\langle 110\rangle$ in TaC(011), are active at room temperature, and that TaC(100) is softer than TaC(011). Our results augment the existing knowledge derived from indentation experiments and provide new insights into the room-temperature deformation mechanisms operating in TMCs.

S.K. and J.M.Y. thank the AFOSR (Dr. Ali Sayir) for Grant # FA9550-10-1-0496. C.R. gratefully acknowledges support from the NSF through Grant # DMS-0931852. The in situ electron microscopy experiments are conducted as part of a user project at the National Center for Electron Microscopy, Lawrence Berkeley National Laboratory, supported by the Office of Science, Office of Basic Energy Sciences, of the U.S. Department of Energy under Contract No. DE-AC02-05CH11231.

[1] L.E. Toth, Transition Metal Carbides and Nitrides, Academic Press, New York, 1971.
[2] G.E. Hollox, Mater. Sci. Eng. 3 (1968) 121–137.
[3] W.S. Williams, Prog. Solid State Chem. 6 (1971) 57–118.
[4] A. Kelly, D. Rowcliffe, J. Am. Ceram. Soc. 50 (1967) 253–256.
[5] H.A. Johansen, J.G. Cleary, J. Electrochem. Soc. 113 (1966) 378–381.
[6] N. De Leon, B. Wang, C.R. Weinberger, L.E. Matson, G.B. Thompson, Acta Mater. 61 (2013) 3905–3913.
[7] D.J. Rowcliffe, G.E. Hollox, J. Mater. Sci. 6 (1971) 1261–1269.
[8] D.J. Rowcliffe, W.J. Warren, J. Mater. Sci. 5 (1970) 345–350.
[9] C. Kim, G. Gottstein, D.S. Grummon, Acta Metall. Mater. 42 (1994) 2291–2301.
[10] Y. Kumashiro, Y. Nagai, H. Katō, J. Mater. Sci. Lett. 1 (1982) 49–52.
[11] D. Lahiri, V. Singh, G.R. Rodrigues, T.M.H. Costa, M.R. Gallas, S.R. Bakshi, S. Seal, A. Agarwal, Acta Mater. 61 (2013) 4001–4009.
[12] S. Kiani, K.W.K. Leung, V. Radmilovic, A.M. Minor, J.-M. Yang, D.H. Warner, S. Kodambaka, Acta Mater., 2014 (in press). Q4
[13] V. Havu, V. Blum, P. Havu, M. Scheffler, J. Comput. Phys. 228 (2009) 8367–8379.
[14] J.P. Perdew, K. Burke, M. Ernzerhof, Phys. Rev. Lett. 77 (1996) 3865–3868.
[15] J.R. Rice, J. Mech. Phys. Solids 40 (1992) 239–271.
[16] S. Korte, W. Clegg, Philos. Mag. 91 (2011) 1150–1162.
[17] D. Kiener, C. Motz, G. Dehm, Mater. Sci. Eng., A 505 (2009) 79–87.
[18] O.V. Kuzmin, Y.T. Pei, J.T.M. De Hosson, Microsc. Microanal. 20 (2014) 1581–1584.
[19] S. Kiani, C. Ratsch, S. Kodambaka, A.M. Minor, J.-M. Yang, unpublished data.
[20] S.H. Jhi, J. Ihm, S.G. Louie, M.L. Cohen, Nature 399 (1999) 132–134.
[21] A.E. Gorum, E.R. Parker, J.A. Pask, J. Am. Ceram. Soc. 41 (1958) 161–164.